Draft version June 11, 2025
Typeset using LaTeX default style in AASTeX631

BSN-IV: Light Curve Modeling and Orbital Evolution of the Total-Eclipse Contact Binary EZ Oct

Asma Ababafi,[1] Mehmet Tanriver,[2,3] Atila Poro,[4,5,*] and Eduardo Fernández Lajús[6]

[1] *Independent researcher, Khuzestan, 64615 Dezful, Iran*
[2] *Department of Astronomy and Space Science, Faculty of Science, Erciyes University, Kayseri TR-38039, Türkiye*
[3] *Erciyes University, Astronomy and Space Science Observatory Application and Research Center, Kayseri TR-38039, Türkiye*
[4] *LUX, Observatoire de Paris, CNRS, PSL, 61 Avenue de l'Observatoire, 75014 Paris, France*
[5] *Astronomy Department of the Raderon AI Lab., BC., Burnaby, Canada*
[6] *Instituto de Astrofísica de La Plata (CCT La Plata-CONICET-UNLP), La Plata, Argentina*

ABSTRACT

We present the first detailed multiband (BVR_cI_c and TESS) photometric analysis of the short-period W Ursae Majoris-type contact binary EZ Oct. This study combines ground-based observations conducted at a Southern Hemisphere observatory in Argentina with data from the TESS mission. To investigate the orbital period variations of EZ Oct, times of minima were extracted from this study's observations and gathered from the literature. EZ Oct shows a steadily increasing orbital period consistent with a quadratic trend. We present a new ephemeris and calculate the mass transfer rate in the system. The trend suggests ongoing conservative mass transfer from the less massive to the more massive star. Light curve modeling was performed using the PHOEBE Python code in conjunction with the MCMC approach, and the inclusion of a cold starspot was required to achieve an adequate fit. Absolute parameters were estimated using Gaia DR3 parallax and astrophysical equations. Our analysis shows that EZ Oct is a total-eclipse contact binary with a mass ratio of 1.969, a fillout factor of 0.106, and an inclination of 82.13°. The positions of the component stars on the mass-luminosity and mass-radius diagrams illustrate their evolutionary status. Moreover, we investigated the relationship between orbital period and stellar luminosity in contact binary stars using a sample of 461 systems with $P < 0.5$ days.

Keywords: binaries: eclipsing – binaries: close – stars: individual (EZ Oct)

1. INTRODUCTION

Eclipsing binary systems play a pivotal role in astrophysics, offering essential insights into star formation, internal stellar structure, and the physical as well as evolutionary properties of stars (e.g., Stassun et al. 2009; Southworth 2012; Stassun et al. 2014). Based on Roche lobe geometry, these systems are generally classified into three types: detached, semi-detached, and contact binaries, as originally proposed by Kopal (1959). Among them, W Ursae Majoris (W UMa)-type contact binaries are commonly composed of stars of spectral types F, G, or K, with both components filling their Roche lobes (Van Hamme 1982). When a star fills its Roche lobe, gravitational interaction with its companion facilitates the transfer of mass and energy (Paczyński 1971; Yakut & Eggleton 2005; Paczyński et al. 2006; Zhang et al. 2016).

These systems are characterized by continuous brightness variations and eclipse minima of nearly equal depth, implying that the surface temperatures of the two stars are very similar (Lucy 1968; Lucy 1976). Contact binaries typically exhibit short orbital periods, usually under one day, with the majority ranging from approximately 0.2 to 0.6 days (Dryomova & Svechnikov 2006; Latković et al. 2021). Although all-sky survey data confirm that such systems are quite common Rucinski (2002), many aspects of their origin, structure, and evolution remain poorly understood. This highlights the necessity for more comprehensive theoretical models and targeted observational investigations.

* atila.poro@obspm.fr (AP)

One of the distinctive photometric behaviors frequently observed in contact binary stars is the so-called O'Connell effect, characterized by asymmetrical maxima in the light curve between eclipses (O'Connell 1951). Although its underlying cause remains a subject of active research, several hypotheses have been proposed, most notably the presence of hot or cool spots on the stellar surfaces—features that are often linked to magnetic activity (Liu & Yang 2003).

Contact binary stars are commonly classified into two subtypes: A-type and W-type. This classification is based on the mass and surface temperature of the components. In A-type systems, the more massive star has a higher effective temperature, while in W-type systems, the more massive star is actually cooler. These differences are not limited to thermal structure; they are also linked to the systems' angular momentum evolution and patterns of mass exchange. According to Zhang et al. (2020), the two subtypes likely follow separate evolutionary paths, highlighting the importance of this distinction in the study of contact binaries.

This work presents the results of our first light curve analysis of the EZ Oct binary system and characterizes its physical properties. This work continues the investigation initiated by Poro et al. (2025b), Poro et al. (2025c) and Poro et al. (2025d) presenting new observations and an in-depth analysis of more W UMa-type contact binary systems in the BSN[1] project. The structure of the paper is as follows: Section 2 outlines the selected target binary system, the photometric observations, and the data reduction process. Section 3 presents the times of minima and the new ephemeris of EZ Oct. The photometric light curve analysis is presented in Section 4. Section 5 describes the method used to determine the absolute parameters of the system. Finally, Section 6 provides the discussion and conclusions.

2. TARGET SYSTEM AND OBSERVATION

The EZ Oct (GSC 09517-00107) binary system has an apparent magnitude of $V^{\rm mag}$ =11.57(11)[2] and is located in the southern hemisphere with coordinates R.A.: 15^h 43^m 13.839386^s and Dec: $-86°$ $48'$ $07.227261"$ (J2000). This system is identified as an eclipsing W Ursae Majoris (EW)-type by Otero et al. (2006). Although this system is currently classified as a contact binary in various catalogs and databases, including the Variable Star Index (VSX[3]) database with 0.285878 days orbital period, it was initially identified by the All-Sky Automated Survey for Supernovae (ASAS; Jayasinghe et al. 2018) catalog as a Δ Scuti star with a period of 0.142939 days (Otero et al. 2006). The ASAS catalog has since updated its classification to recognize the system as a contact binary. The VSX and ASAS-SN databases report an orbital period of 0.285878 days and maximum apparent magnitudes of $11.37^{\rm mag}$ and $11.56^{\rm mag}$ in the V band, respectively.

EZ Oct was observed on May 25, 2023, using the 2.15-meter Jorge Sahade Telescope (JS) at the Complejo Astronómico El Leoncito Observatory (CASLEO), located in San Juan, Argentina (69°18′W, 31°48′S; 2552 m above sea level). A total of 926 images were acquired during the observing process. The observations were carried out using a VersArray 2048B CCD camera (Roper Scientific, Princeton Instruments), operated in a 5 × 5 pixel binning mode to enhance the signal-to-noise ratio and reduce readout time. Standard Johnson-Cousins B, V, R_c, and I_c filters were used throughout the observations, with an exposure time of 12 seconds per frame.

The APPHOT photometry package of the Image Reduction and Analysis Facility (IRAF) was used for CCD reduction and aperture photometry Tody 1986. The reduction process incorporated the use of bias and flat-field calibration frames to ensure accurate photometric measurements.

High-quality time-series photometric data from the Transiting Exoplanet Survey Satellite (TESS) was available for EZ Oct (TIC 290410988). The TESS mission primarily aims to identify and categorize exoplanets through systematic observations and data analysis (Ricker et al. 2015). Each TESS sector monitors a designated portion of the sky for approximately 27.4 days. All observational data used in this study were retrieved from the Mikulski Archive for Space Telescopes (MAST)[4]. TESS-like light curves were generated using the LightKurve package[5], and the data were processed to remove trends by applying the TESS Science Processing Operations Center (SPOC) pipeline (Jenkins et al. 2016).

[1] https://bsnp.info/

[2] http://simbad.cds.unistra.fr/simbad

[3] https://www.aavso.org/vsx/

[4] https://mast.stsci.edu/portal/Mashup/Clients/Mast/Portal.htmL

[5] https://docs.lightkurve.org

Table 1. Specifications of the TESS data used in this study.

TESS Sector	Observation Year	Exposure Length	Error Average
12	2019	120	0.0013
13	2019	120	0.0014
65	2023	200	0.0012
66	2023	200	0.0011

Sector 66 was selected for light curve analysis as it contains the most recent available time-series data. To calculate a new ephemeris, observations from all available TESS sectors were incorporated. The TESS sectors used, along with their exposure times and average flux uncertainties, are listed in Table 1.

3. ORBITAL PERIOD VARIATION

In this study, we present a detailed investigation of EZ Oct using updated and available data. We compiled as many times of minima as possible from photometric surveys to support the analysis of orbital period variations in the system. Since the dataset included both Barycentric Julian Dates in Barycentric Dynamical Time (BJD_{TDB}) and Heliocentric Julian Dates (HJD), we first standardized all entries to BJD_{TDB} using an online conversion tool[6]. Primary and secondary times of minima were extracted from our own observations across the filters used, as well as from the available TESS time-series data. The times of minima derived from our observations are listed in Table 2, while a machine-readable version of the minima extracted from the TESS data is also provided online.

To calculate the epoch and observed-minus-calculated (O-C) values for each eclipse time, we used the orbital period of 0.285878 days from the VSX database, adopting the minimum time from our observation as the reference ephemeris (Table 2 and a machine-readable version table).

The O-C diagram is a fundamental tool for diagnosing orbital period variations in eclipsing binary systems. For the EZ Oct system, we constructed a detailed O-C diagram based on eclipse timing data collected over several years. This extensive dataset incorporates high-precision measurements from both space-based missions, notably TESS, and complementary ground-based photometric observations. The resulting temporal baseline enables a sensitive probe of small-scale orbital variations, providing critical insight into the system's dynamical evolution.

Analysis of the O-C diagram for EZ Oct revealed a pronounced upward curvature, indicative of a sustained secular increase in its orbital period. To quantify this behavior, a quadratic least-squares fit was applied to the eclipse timing data using the ephemeris equation:

$$O - C = aE^2 + bE + c \tag{1}$$

where E is the epoch number, and a, b, and c are the fitted coefficients. Hence, the quadratic ephemeris of EZ Oct is expressed as:

$$T_{min} = T_0 + P_0 E + aE^2 \tag{2}$$

where T_0 and P_O are come from the reference epoch, and a represents the quadratic period variation coefficient.

The following light elements were assigned to a new ephemeris for the minima obtained from this study, TESS, and the literature:

$$BJD_{TDB}(Min.I) = 2460089.60443(25) + 0.28587864(63) \times E \tag{3}$$

where E is the integer number of orbital cycles after the reference epoch.

Moreover, the instantaneous period change rate is defined by:

$$\dot{P} \approx \frac{dP}{dE}.\frac{dE}{dt} = 2aP_0 \tag{4}$$

[6] https://astroutils.astronomy.osu.edu/time/hjd2bjd.html

Table 2. Extracted and collected times of minima.

Min.(BJD_{TDB})	Error	Epoch	O-C(day)	Filter	Reference
2457504.12354		-9044.0	-0.00535	V	VarAstro[a]
2457504.26648		-9043.5	-0.00499	V	VarAstro
2458138.05800		-6826.5	-0.00416	V	ASAS-SN
2460089.60403	0.00015	0.0	-0.00014	R	This study
2460089.60417	0.00019	0.0	0.00000	V	This study
2460089.60436	0.00028	0.0	0.00019	I	This study
2460089.60491	0.00022	0.0	0.00074	B	This study
2460089.74759	0.00011	0.5	0.00048	V	This study
2460089.74762	0.00008	0.5	0.00051	I	This study
2460089.74776	0.00007	0.5	0.00065	B	This study
2460089.74780	0.00011	0.5	0.00069	R	This study

[a] http://var2.astro.cz/ocgate/

Substituting the best-fit coefficients yields a value of $\dot{P} \approx 1.090 \times 10^{-3}$ sec/year.

This statistically significant positive period derivative is consistent with theoretical expectations for conservative mass transfer from the lower-mass component to the more massive star, resulting in an expanding orbital separation and increasing orbital period (Yakut & Eggleton 2005).

It is worth noting that no significant cyclic modulation was detected in the O–C residuals beyond the fitted parabolic trend. This suggests that if a third body is present, it either has a long orbital period beyond the current observational baseline or exerts negligible dynamical influence on the inner binary. Additionally, there is no strong evidence for short-term variations due to magnetic activity cycles (e.g., the Applegate mechanism, Applegate 1992), though such effects may become apparent with higher-cadence, long-term observations in the future.

4. LIGHT CURVE SOLUTION

We employed version 2.4.9 of the PHysics Of Eclipsing BinariEs (PHOEBE; Prša et al. 2016, Conroy et al. 2020) Python package to analyze the photometric light curves of the EZ Oct binary system. The observation times in the light curves were converted into orbital phases based on the reference ephemeris provided in Section 3. Given the morphology of the observed light curves, the systems' classifications in the catalogs, and their relatively short orbital periods, the contact binary configuration was selected for the modeling process. The gravity darkening parameter was fixed at $g_1 = g_2 = 0.32$ (Lucy 1967), while the bolometric albedo was set to $A_1 = A_2 = 0.5$ (Ruciński 1969). Stellar atmospheres were modeled using the approach described by Castelli & Kurucz (2004), and the limb darkening coefficients were left as adjustable parameters within PHOEBE.

The initial effective temperature (T) used in the analysis was obtained from the Gaia DR3 catalog, which reports a value of 5025 K for this system. This temperature corresponds to the hotter component, as determined from the depth of the light curve minima. The effective temperature of the cooler star was initially estimated by estimating the difference in depth between the primary and secondary minima in the light curves.

The initial mass ratio of the EZ Oct binary system was estimated using the q-search technique (Terrell & Wilson 2005). A broad range of mass ratio values from 0.1 to 12 was examined during the q-search. This was followed by a more focused search within a narrower interval to refine the result by minimizing the sum of squared residuals. As shown in Figure 2, the q-search curve display a distinct minimum, indicating the most likely solution. Previous studies, such as those by Li et al. (2021) and Poro et al. (2024b), have demonstrated that systems with high orbital inclinations and total eclipses yield reliable mass ratio determinations.

The analysis reveals that EZ Oct displays unequal maxima in its light curve. To account for this asymmetry in the light curve solution process, a cool starspot was required on one of the stellar components. This feature is most likely the result of magnetic activity, which leads to the formation of starspots and manifests as the well-known O'Connell effect (O'Connell 1951, Sriram et al. 2017). The parameters used to describe the starspot, including colatitude (Col.°), longitude (Long.°), angular radius (Radius°), and the temperature ratio (T_{spot}/T_{star}), are listed in Table 3.

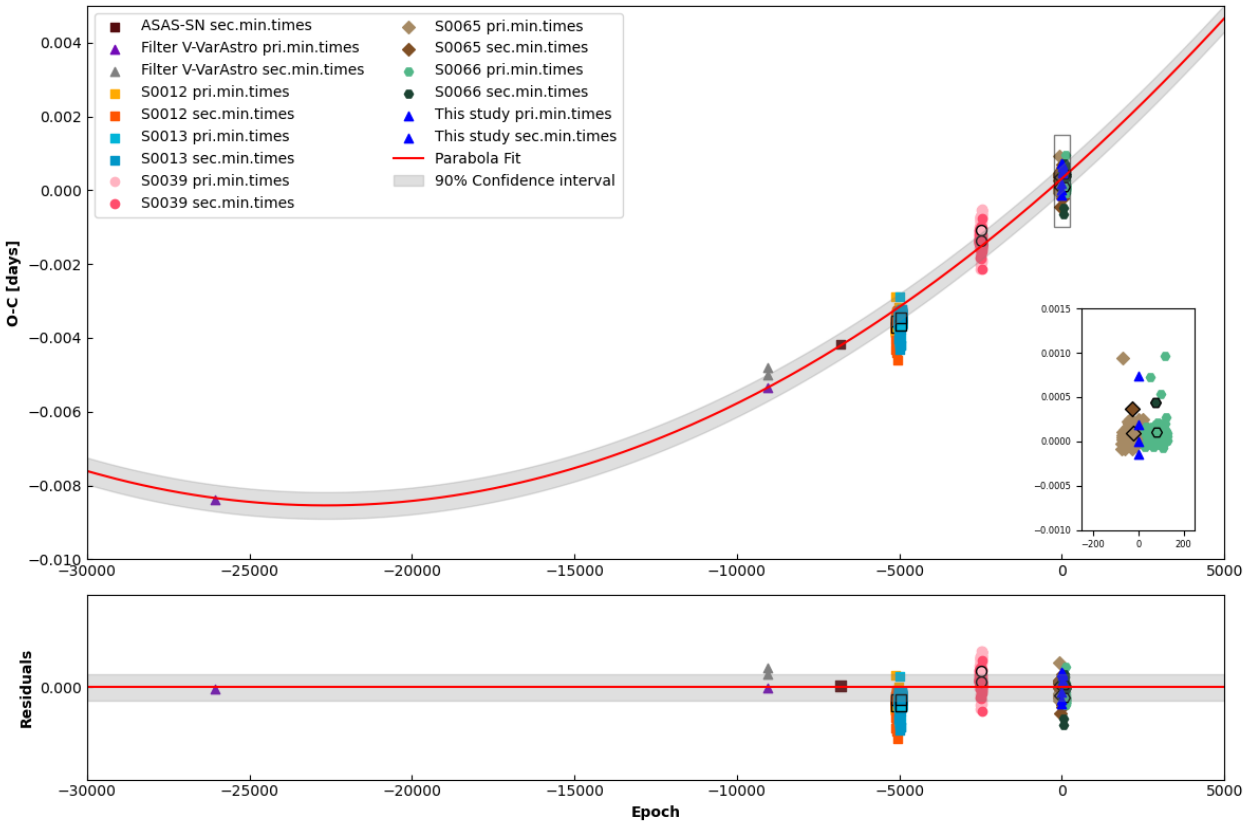

Figure 1. The O-C diagram of the EZ Oct systems.

Photometric multiband data, along with the initial parameter values, were then used to obtain a satisfactory theoretical fit to the observed light curve. The optimization tool in PHOEBE was subsequently applied to further refine the solution and improve the accuracy of the light curve modeling.

To determine the final parameter values and their associated uncertainties, we applied the Markov Chain Monte Carlo (MCMC) method using the emcee package (Foreman-Mackey et al. 2013). The five key parameters included in the MCMC modeling were the mass ratio (q), orbital inclination (i), fillout factor (f), and the effective temperatures of both stellar components (T_1 and T_2). A Gaussian likelihood function was adopted to represent the observational light curve comprehensively. The sampling was carried out using 32 walkers over 1000 iterations, with the initial 300 steps discarded as burn-in. The results of the light curve analysis showed no evidence of a third light contribution (l_3) in any of the systems studied.

The results of the light curve analysis for EZ Oct are summarized in Table 3. The corresponding corner plot is shown in Figure 3. Figure 4 presents the final synthetic light curves overlaid with the observed data for the binary systems. Additionally, three-dimensional representations of the systems are illustrated in Figure 5.

5. FUNDAMENTAL PARAMETERS

We estimated the absolute parameters of the target system using the parallax reported in Gaia DR3 (Poro et al. 2024c). This approach is considered reliable when photometric observations are available, due to the high precision of Gaia DR3 parallaxes (Li et al. 2021). However, to ensure the validity of this method, certain conditions must be met: the visual extinction coefficient (A_V) should be less than approximately 0.4 (Poro et al. 2024a), and the Renormalized Unit Weight Error (RUWE) must not exceed 1.4 (Lindegren et al. 2018). For the EZ Oct system, both criteria are satisfied. We determined $A_V = 0.220 \pm 0.001$ using the 3D dust map by Green et al. (2019), and the RUWE value was taken directly from the Gaia DR3 archive. Additionally, we adopted $V_{\max} = 11.57 \pm 0.04$ comes from our observations as the system's apparent brightness at maximum light.

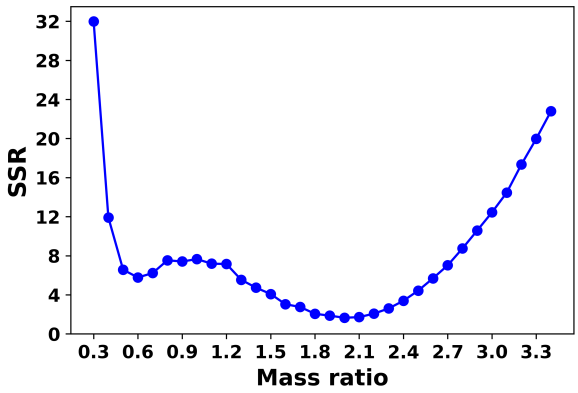

Figure 2. Sum of the squared residuals as a function of the mass ratio.

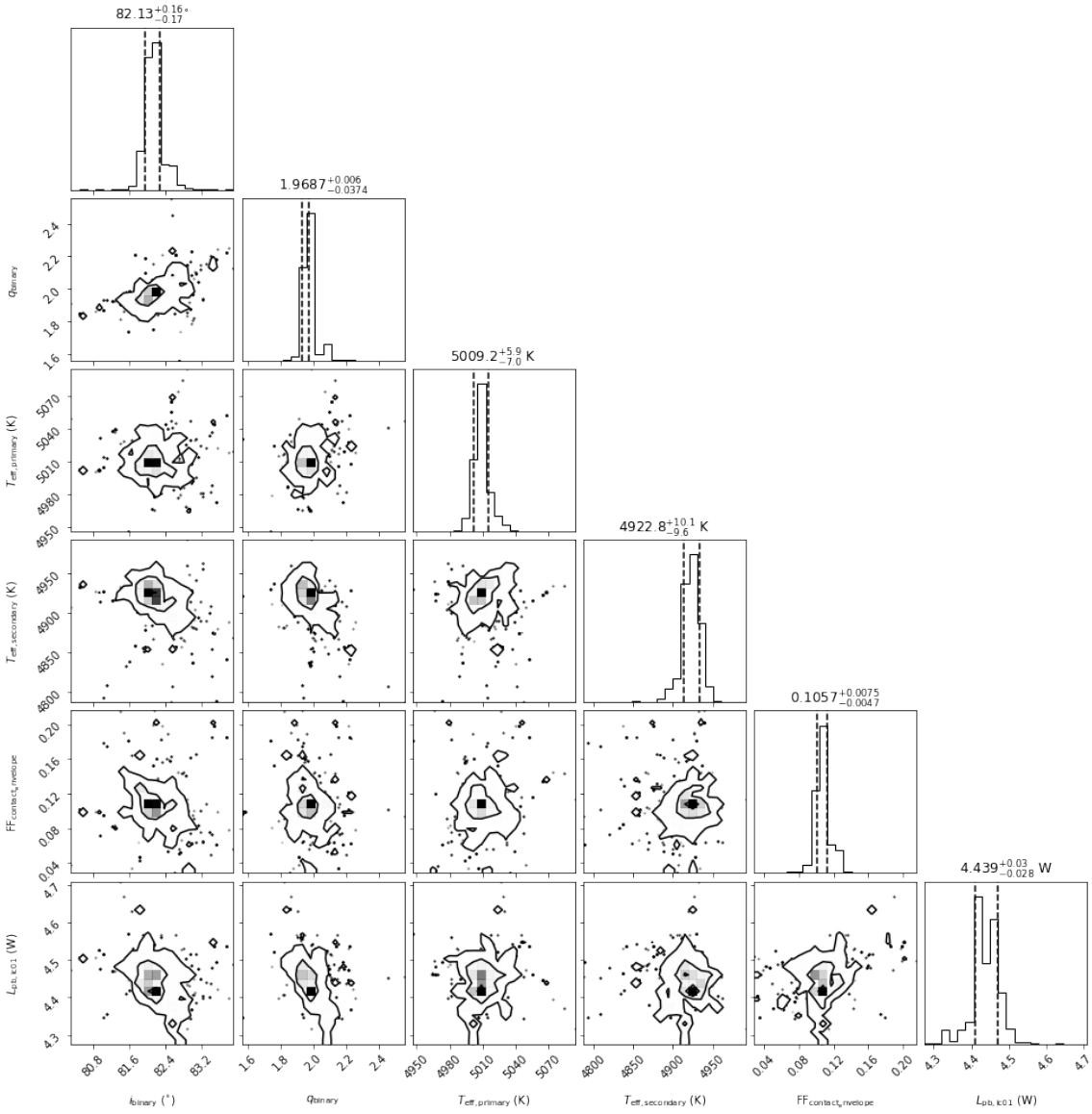

Figure 3. The corner plots of the target system were determined by MCMC modeling.

Table 3. Light curve analysis of EZ Oct.

Parameter	Result	Parameter	Result
T_1 (K)	5009^{+6}_{-7}	$r_{1(mean)}$	0.330 ± 0.008
T_2 (K)	4923^{+10}_{-10}	$r_{2(mean)}$	0.448 ± 0.007
$q = M_2/M_1$	$1.969^{+0.006}_{-0.037}$	Phase shift	0.024
f	$0.106^{+0.008}_{-0.005}$	Colatitude$_{spot}$(deg)	71
i°	$82.13^{+0.16}_{-0.17}$	Longitude$_{spot}$(deg)	254
$\Omega_1 = \Omega_2$	5.145 ± 0.063	Radius$_{spot}$(deg)	20
l_1/l_{tot}	$0.375^{+0.002}_{-0.002}$	T_{spot}/T_{star}	0.89
l_2/l_{tot}	0.625 ± 0.002	Component$_{spot}$	Secondary

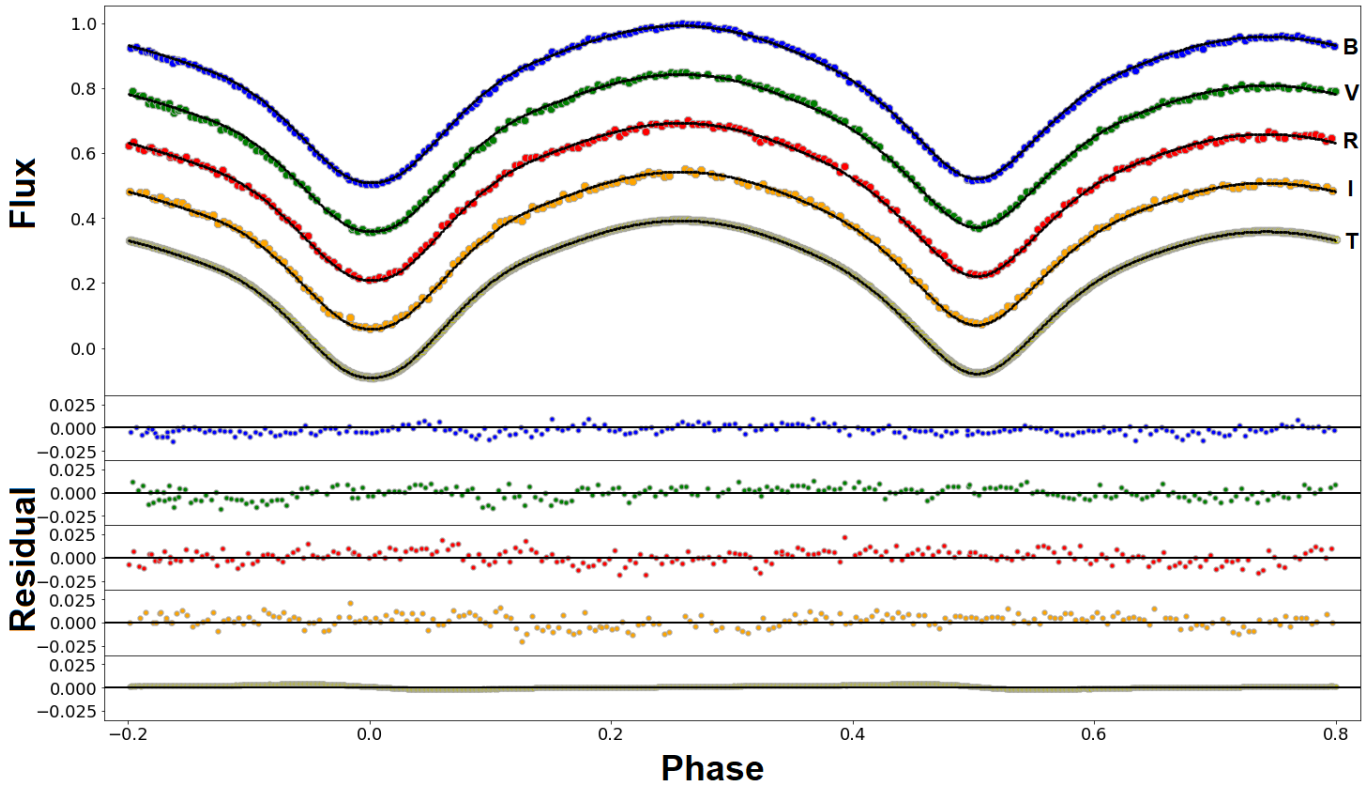

Figure 4. Colored dots represent the observed light curves of the systems in different filters (from top to bottom: B, V, R_c, I_c, TESS), while the corresponding synthetic light curves, computed from the light curve solutions, are shown as solid lines.

First, we estimated the system's absolute visual magnitude (M_V) using the apparent magnitude (V), the distance derived from Gaia DR3, and the visual extinction A_V. Subsequently, the individual absolute magnitudes of the components, M_{V1} and M_{V2}, were determined using the light ratio in the V-band ($l_{1,2}/l_{\rm tot}$) obtained from the light curve solution. The absolute bolometric magnitudes ($M_{\rm bol1,2}$) were then calculated by applying bolometric corrections ($BC_{1,2}$) taken from the study by Flower 1996. The radii of the binary components were derived from the bolometric magnitudes and the corresponding luminosities (L). In this calculation, we adopted a solar bolometric magnitude of $M_{\rm bol\odot} = 4.73$ mag, following Torres 2010. With the luminosity estimated in this way and the effective temperatures obtained from the light curve analysis, the stellar radii (R) were computed. The semi-major axis $a(R_\odot)$ was determined

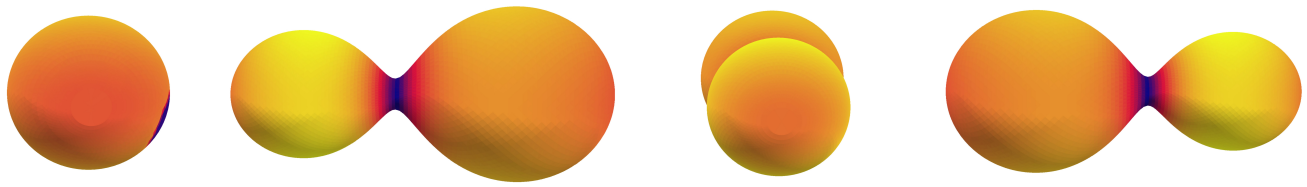

Figure 5. Three-dimensional views of the stars in the target binary system at orbital phases 0, 0.25, 0.5 and 0.75, respectively. The colors represent variations in surface temperature based on model simulations, with darker tones indicating cooler regions and lighter areas corresponding to higher temperatures.

Table 4. Estimation of absolute parameters.

Parameter	Hotter star	Cooler star
$M(M_\odot)$	0.454 ± 0.006	0.895 ± 0.011
$R(R_\odot)$	0.665 ± 0.015	0.906 ± 0.024
$L(L_\odot)$	0.250 ± 0.010	0.433 ± 0.019
$M_{bol}(mag)$	6.245 ± 0.043	5.65 ± 0.048
$log(g)(cgs)$	4.449 ± 0.025	4.476 ± 0.028
$a(R_\odot)$	2.018 ± 0.008	
$BC(mag)$	-0.304 ± 0.003	-0.344 ± 0.005

using the radii $R_{1,2}$ and the mean relative radii $r_{\text{mean1,2}}$, by averaging the resulting values of $a_1(R_\odot)$ and $a_2(R_\odot)$. Finally, with the known parameters $a(R_\odot)$, orbital period P_{orb}, and mass ratio q, the individual stellar masses were estimated using Kepler's third law (Equations 5, 6).

$$M_1 = \frac{4\pi^2 a^3}{GP^2(1+q)} \tag{5}$$

$$M_2 = q \times M_1 \tag{6}$$

The orbital angular momentum (J_0) of the system was computed using Equation 7, as described in the study by Eker et al. 2006, based on the total mass, mass ratio (q), and orbital period (P) of the system. The calculated value of J_0 is 51.48 ± 0.01 (in units of $g.cm^2/s$). This output means EZ Oct is in a contact binary systems region.

$$J_0 = \frac{q}{(1+q)^2} \sqrt[3]{\frac{G^2}{2\pi} M^5 P} \tag{7}$$

The derived absolute parameters for EZ Oct are presented in Table 4.

6. DISCUSSION AND CONCLUSION

In this study, we present a comprehensive photometric analysis of the contact binary system EZ Oct, including an investigation of orbital period variations, light curve modeling, and the estimation of absolute parameters. The data were obtained through multiband photometric observations conducted at an observatory in Argentina. Based on the results, the following discussion and conclusions are presented:

A) A defining characteristic of overcontact binary systems such as EZ Oct is the sustained and dynamically significant mass exchange between their stellar components. This process is a key driver of orbital evolution, influencing both the orbital period and the system's angular momentum budget, and ultimately steering the binary toward a coalescence phase.

Assuming conservative mass transfer—in which no mass escapes the system—the rate of orbital period variation is directly linked to the mass transfer rate via the following relation (Hilditch 2001):

$$\frac{\dot{P}}{P} = -3\dot{M}(\frac{1}{M_1} - \frac{1}{M_2}). \tag{8}$$

Using this relation, we estimate the mass transfer rate as $\dot{M} = 1.353 \times 10^{-8}\ M_\odot$/year.

This substantial rate indicates rapid mass redistribution from the less massive primary to the more massive secondary. Under conservative conditions, such mass flow increases the orbital separation and period, consistent with the upward curvature observed in the O–C diagram.

B) In the contact binary system EZ Oct, the observed asymmetry between the two light curve maxima, which is a signature of the O'Connell effect (O'Connell 1951), required the addition of a cool starspot on one of the stellar components in order to achieve a satisfactory fit. Moreover, the light curve solution indicates a temperature difference of 86 K between the two stellar components. The final effective temperature of EZ Oct, derived using an initial value from Gaia DR3, is consistent with the overall correlation between Gaia-based temperatures and model-derived values as investigated by Poro et al. (2025b). The spectral classifications of the stars were determined based on the temperature criteria outlined by Cox (2000) and Eker et al. (2018). Accordingly, the stellar components of EZ Oct are classified as K1 and K2 spectral types based on their effective temperatures.

C) In contact binary systems, the extent of envelope sharing between the stellar components is described by the fillout factor (f), which quantifies how much the stars overfill their Roche lobes and merge into a common envelope. This parameter serves as a key indicator of the degree of contact, offering insight into the efficiency of mass and energy exchange within the system. Binaries with small f values are typically in a shallow contact configuration, where the shared envelope is limited, while larger values reflect deeper levels of interaction and more significant overcontact. The fillout factor is calculated using the following expression:

$$f = \frac{\Omega - \Omega_{\rm in}}{\Omega_{\rm out} - \Omega_{\rm in}}, \tag{9}$$

where Ω denotes the effective surface potential of the system, and $\Omega_{\rm in}$ and $\Omega_{\rm out}$ represent the inner and outer critical potentials, respectively, as defined by Mochnacki (1981).

Based on the value of the fillout factor (f), contact binary systems are typically classified into three categories: shallow ($f < 25\%$), medium ($25\% \leq f < 50\%$), and deep contact systems ($f \geq 50\%$) (Li et al. 2022). According to the light curve solution, EZ Oct falls into the shallow contact category.

D) Since all required conditions were met, the Gaia DR3 parallax was used to estimate the system's absolute parameters. In this approach, the paths of the primary and secondary stars are treated independently, yielding $a_1(R_\odot) = 2.015$ and $a_2(R_\odot) = 2.022$ as their respective semi-major axes. The computed values show good agreement, with a difference of only $\Delta a = |a_2 - a_1| = 0.007$, which supports the validity of the method. This Δa value further confirms the reliability of the light curve solution and the adopted model parameters (Poro et al. 2024c, 2025a).

E) The evolutionary status of EZ Oct is shown using logarithmic Mass-Radius (M-R) and Mass-Luminosity (M-L) diagrams, constructed from its derived absolute parameters (Table 4, Figure 6). In these diagrams, the two stellar components are plotted relative to the Zero-Age Main Sequence (ZAMS) and Terminal-Age Main Sequence (TAMS) lines, as defined by Girardi et al. (2000), which illustrates their positions along the stellar evolutionary path.

Based on the light curve modeling and the estimated absolute parameters, the less massive component of EZ Oct is determined to be hotter than its companion. As illustrated in Figure 6, the lower-mass star is located near the TAMS, while the more massive component lies closer to the ZAMS, indicating that the two stars are at distinct evolutionary stages along the main sequence.

F) In this study, the system EZ Oct was identified as a W UMa-type contact eclipsing binary. The light curve analysis, based on parameters such as mass ratio, fillout factor, and orbital inclination, confirms its contact binary nature. According to the classification criteria for A and W subtypes of contact binaries defined by Binnendijk (1970), and based on the derived temperatures and masses of the components, EZ Oct is classified as a W-subtype contact system. In such systems, the less massive star is hotter than its companion, which is consistent with the physical characteristics of EZ Oct.

G) The period–luminosity (P–L) relationship in W UMa-type contact binaries has been extensively investigated following the study by Eggen (1967). Rucinski (1994) introduced a period–luminosity–color (PLC) relation based on 18 systems, which was subsequently refined by Rucinski & Duerbeck (1997) through the use of HIPPARCOS parallaxes and an expanded sample of 40 binaries. However, later studies (e.g., Rucinski 2006; Muraveva et al. 2014; Pawlak

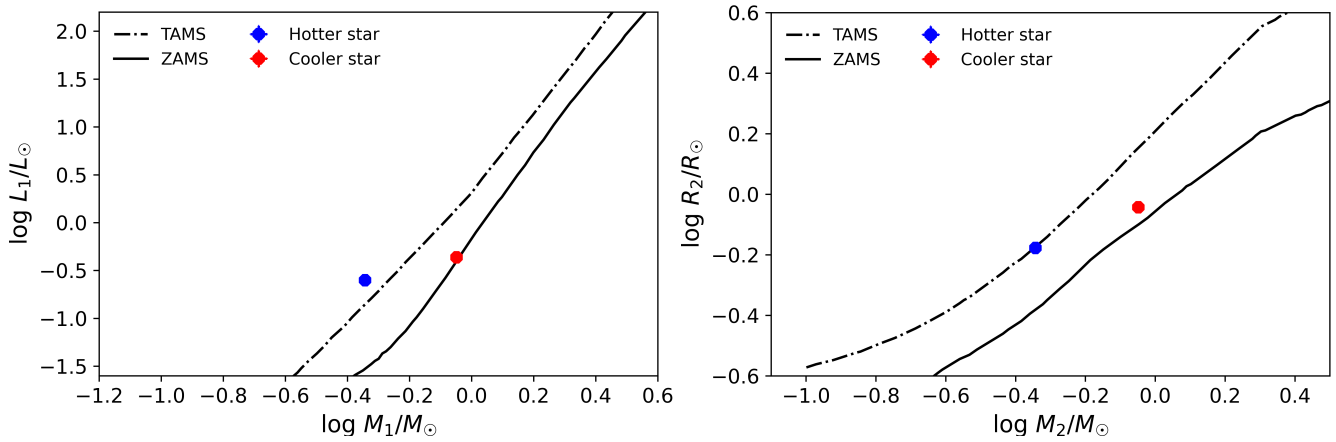

Figure 6. Logarithmic Mass-Radius and Mass-Luminosity diagrams of EZ Oct components relative to ZAMS and TAMS lines.

2016) yielded mixed results, often constrained by limited sample sizes or uncorrected period–color correlations. A more robust P–L relation with approximately 10% accuracy was presented by Chen et al. (2016), using a sample of 66 contact binaries. Building on this, Chen et al. (2018) employed 183 nearby systems with precise TGAS parallaxes and included both optical and mid-infrared photometry. Then, Latković et al. (2021) analyzed 210 W UMa-type systems with orbital periods below 0.5 days, deriving distinct P–L relations for the primary and secondary components (Equation 10). More recently, Poro et al. (2024d) investigated the P–L relationship using a sample of 118 contact systems, with luminosities estimated via a method based on Gaia DR3 parallaxes. They provided revised P–L relations separately for the primary and secondary components (Equation 11).

$$\left.\begin{aligned}\log L_1 &= (13.98 \pm 0.75)P - (3.04 \pm 0.27)\\ \log L_2 &= (3.66 \pm 0.26)P - (0.69 \pm 0.09)\end{aligned}\right\} \quad \text{Latković et al. (2021)} \tag{10}$$

$$\left.\begin{aligned}\log L_1 &= (4.15 \pm 0.11)\ \log P + (1.90 \pm 0.13)\\ \log L_2 &= (2.82 \pm 0.12)\ \log P + (1.08 \pm 0.15)\end{aligned}\right\} \quad \text{Poro et al. (2024d)} \tag{11}$$

This investigation revisits the empirical P–L parameter relationship using an expanded dataset from the Poro et al. (2025a) study, exceeding the sample sizes of previous studies. Our sample includes 461 contact systems with orbital periods shorter than 0.5 days. A linear fit was applied to the data, as shown in Figure 7, to examine the overall trend of the P–L relationship. A heatmap was also overlaid on the diagrams to illustrate the density distribution of the systems across the parameter space. The position of the EZ Oct system is marked on the diagrams, and the revised P–L_1 and P–L_2 relations are presented as follows (Equations 12, 13):

$$logL_1 = (3.79 \pm 0.10) \times logP + (1.89 \pm 0.05), \tag{12}$$

$$logL_2 = (2.78 \pm 0.11) \times logP + (0.99 \pm 0.05). \tag{13}$$

DATA AVAILABILITY

Ground-based data and extracted minima are available in the paper's online supplement.

ACKNOWLEDGMENTS

This manuscript, including the observation, analysis, and writing processes, was provided by the BSN project. We used results from the European Space Agency mission Gaia[7]. This research did not receive any specific grant from

[7] http://www.cosmos.esa.int/gaia

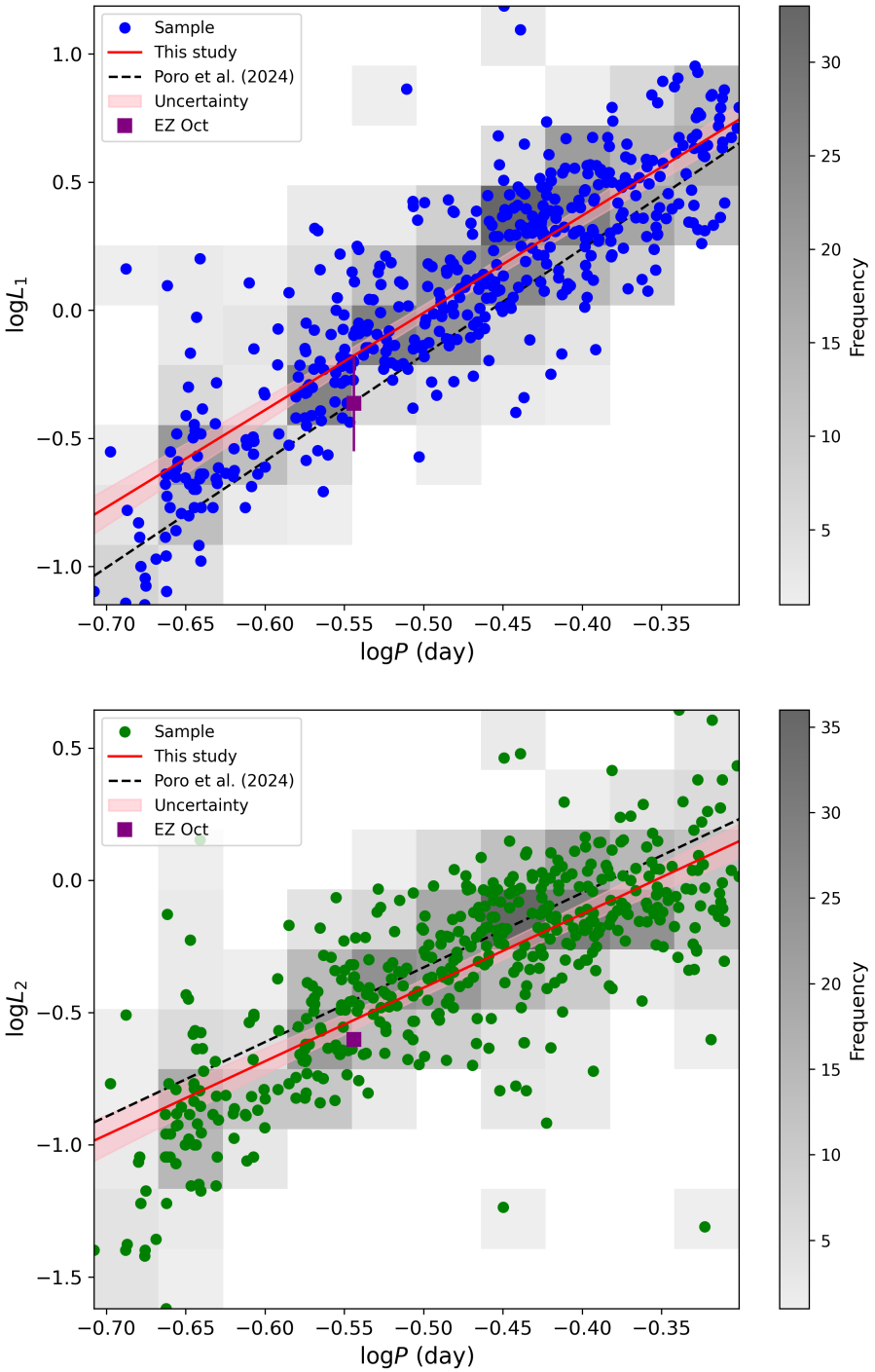

Figure 7. Two-dimensional relationships between orbital period and luminosity for component stars in W UMa-type contact binary systems.

funding agencies in the public, commercial, or not-for-profit sectors. We used IRAF, which is distributed by the National Optical Observatories and operated by the Association of Universities for Research in Astronomy, Inc., under a cooperative agreement with the National Science Foundation.

ORCID IDS

Asma Ababafi: 0009-0004-8579-7692
Mehmet Tanriver: 0000-0002-3263-9680
Atila Poro: 0000-0002-0196-9732
Eduardo Fernández Lajús: 0000-0002-9262-4456

REFERENCES

Applegate, J. H. 1992, ApJ, 385, 621, doi: 10.1086/170967
Binnendijk, L. 1970, Vistas in Astronomy, 12, 217, doi: 10.1016/0083-6656(70)90041-3
Castelli, F., & Kurucz, R. L. 2004, A&A, 419, 725, doi: 10.1051/0004-6361:20040079
Chen, X., de Grijs, R., & Deng, L. 2016, ApJ, 832, 138, doi: 10.3847/0004-637X/832/2/138
Chen, X., Deng, L., de Grijs, R., Wang, S., & Feng, Y. 2018, ApJ, 859, 140, doi: 10.3847/1538-4357/aabe83
Conroy, K. E., Kochoska, A., Hey, D., et al. 2020, ApJS, 250, 34, doi: 10.3847/1538-4365/abb4e2
Cox, A. N. 2000, Allen's astrophysical quantities (New York: AIP Press; Springer; Editedy by Arthur N. Cox.)
Dryomova, G. N., & Svechnikov, M. A. 2006, Astrophysics, 49, 358, doi: 10.1007/s10511-006-0036-9
Eggen, O. J. 1967, MmRAS, 70, 111
Eker, Z., Demircan, O., Bilir, S., & Karataş, Y. 2006, MNRAS, 373, 1483, doi: 10.1111/j.1365-2966.2006.11073.x
Eker, Z., Bakış, V., Bilir, S., et al. 2018, MNRAS, 479, 5491, doi: 10.1093/mnras/sty1834
Flower, P. J. 1996, ApJ, 469, 355, doi: 10.1086/177785
Foreman-Mackey, D., Hogg, D. W., Lang, D., & Goodman, J. 2013, PASP, 125, 306, doi: 10.1086/670067
Girardi, L., Bressan, A., Bertelli, G., & Chiosi, C. 2000, A&AS, 141, 371, doi: 10.1051/aas:2000126
Green, G. M., Schlafly, E., Zucker, C., Speagle, J. S., & Finkbeiner, D. 2019, ApJ, 887, 93, doi: 10.3847/1538-4357/ab5362
Hilditch, R. W. 2001, An Introduction to Close Binary Stars (Cambridge, UK: Cambridge University Press)
Jayasinghe, T., Kochanek, C. S., Stanek, K. Z., et al. 2018, MNRAS, 477, 3145, doi: 10.1093/mnras/sty838
Jenkins, J. M., Twicken, J. D., McCauliff, S., et al. 2016, in Society of Photo-Optical Instrumentation Engineers (SPIE) Conference Series, Vol. 9913, Software and Cyberinfrastructure for Astronomy IV, ed. G. Chiozzi & J. C. Guzman, 99133E, doi: 10.1117/12.2233418
Kopal, Z. 1959, Close binary systems (The International Astrophysics Series, London: Chapman and Hall)
Latković, O., Čeki, A., & Lazarević, S. 2021, ApJS, 254, 10, doi: 10.3847/1538-4365/abeb23
Li, K., Gao, X., Liu, X.-Y., et al. 2022, AJ, 164, 202, doi: 10.3847/1538-3881/ac8ff2
Li, K., Xia, Q.-Q., Kim, C.-H., et al. 2021, AJ, 162, 13, doi: 10.3847/1538-3881/abfc53
Lindegren, L., et al. 2018, Gaia Technical Note: GAIA-C3-TN-LU-LL-124-01
Liu, Q.-Y., & Yang, Y.-L. 2003, ChJA&A, 3, 142, doi: 10.1088/1009-9271/3/2/142
Lucy, L. 1968, ApJ, 151, 1123, doi: 10.1086/149510
—. 1976, ApJ, 205, 208, doi: 10.1086/154265
Lucy, L. B. 1967, ZA, 65, 89
Mochnacki, S. W. 1981, ApJ, 245, 650, doi: 10.1086/158845
Muraveva, T., Clementini, G., Maceroni, C., et al. 2014, MNRAS, 443, 432, doi: 10.1093/mnras/stu1151
O'Connell, D. J. K. 1951, Publications of the Riverview College Observatory, 2, 85
Otero, S. A., Hoogeveen, G. J., & Wils, P. 2006, Information Bulletin on Variable Stars, 5674, 1
Paczyński, B. 1971, ARA&A, 9, 183, doi: 10.1146/annurev.aa.09.090171.001151
Paczyński, B., Szczygieł, D. M., Pilecki, B., & Pojmański, G. 2006, MNRAS, 368, 1311, doi: 10.1111/j.1365-2966.2006.10223.x
Pawlak, M. 2016, MNRAS, 457, 4323, doi: 10.1093/mnras/stw269
Poro, A., Jahangiri, E., Sarvari, E., et al. 2025a, MNRAS, 538, 1427, doi: 10.1093/mnras/staf356
Poro, A., Tanriver, M., Michel, R., & Paki, E. 2024a, PASP, 136, 024201, doi: 10.1088/1538-3873/ad1ed3
Poro, A., Li, K., Michel, R., et al. 2024b, AJ, 168, 272, doi: 10.3847/1538-3881/ad8345
Poro, A., Hedayatjoo, M., Nastaran, M., et al. 2024c, NewA, 110, 102227, doi: 10.1016/j.newast.2024.102227
Poro, A., Paki, E., Alizadehsabegh, A., et al. 2024d, Research in Astronomy and Astrophysics, 24, 015002, doi: 10.1088/1674-4527/ad0866
Poro, A., Li, K., Paki, E., et al. 2025b, MNRAS, 537, 3160, doi: 10.1093/mnras/staf222

Poro, A., Li, K., , et al. 2025c, AJ, Under review
—. 2025d, PASP, Under review
Prša, A., Conroy, K. E., Horvat, M., et al. 2016, ApJS, 227, 29, doi: 10.3847/1538-4365/227/2/29
Ricker, G. R., Winn, J. N., Vanderspek, R., et al. 2015, Journal of Astronomical Telescopes, Instruments, and Systems, 1, 014003, doi: 10.1117/1.JATIS.1.1.014003
Rucinski, S. 2002, PASP, 114, 1124, doi: 10.1086/342677
—. 2006, MNRAS, 368, 1319, doi: 10.1111/j.1365-2966.2006.10207.x
Ruciński, S. M. 1969, AcA, 19, 245
Rucinski, S. M. 1994, PASP, 106, 462, doi: 10.1086/133401
Rucinski, S. M., & Duerbeck, H. W. 1997, PASP, 109, 1340, doi: 10.1086/134014
Southworth, J. 2012, in Orbital Couples: Pas de Deux in the Solar System and the Milky Way, ed. F. Arenou & D. Hestroffer, 51–58, doi: 10.48550/arXiv.1201.1388
Sriram, K., Malu, S., Choi, C. S., & Vivekananda Rao, P. 2017, AJ, 153, 231, doi: 10.3847/1538-3881/aa6893
Stassun, K. G., Feiden, G. A., & Torres, G. 2014, NewAR, 60, 1, doi: 10.1016/j.newar.2014.06.001
Stassun, K. G., Hebb, L., López-Morales, M., & Prša, A. 2009, in IAU Symposium, Vol. 258, The Ages of Stars, ed. E. E. Mamajek, D. R. Soderblom, & R. F. G. Wyse, 161–170, doi: 10.1017/S1743921309031810
Terrell, D., & Wilson, R. E. 2005, Ap&SS, 296, 221, doi: 10.1007/s10509-005-4449-4
Tody, D. 1986, in Society of Photo-Optical Instrumentation Engineers (SPIE) Conference Series, Vol. 627, Instrumentation in astronomy VI, ed. D. L. Crawford, 733, doi: 10.1117/12.968154
Torres, G. 2010, AJ, 140, 1158, doi: 10.1088/0004-6256/140/5/1158
Van Hamme, W. 1982, Astronomy and Astrophysics, 105, 389
Yakut, K., & Eggleton, P. P. 2005, ApJ, 629, 1055, doi: 10.1086/431300
Zhang, X.-D., Qian, S.-B., & Liao, W.-P. 2020, MNRAS, 492, 4112, doi: 10.1093/mnras/staa079
Zhang, Y., Han, Q. W., & Liu, J. Z. 2016, PASP, 128, 124201, doi: 10.1088/1538-3873/128/970/124201